Computer Vision-Based Technique to Measure Displacement in Selected Soil Tests

Article *in* Geotechnical Testing Journal · March 1998

DOI: 10.1520/GTJ10422J

CITATIONS
8

READS
190

4 authors, including:

Ronald Chaney
Humboldt State University
274 PUBLICATIONS **7,225** CITATIONS
SEE PROFILE

Kenneth R. Demars
University of Connecticut
262 PUBLICATIONS **7,488** CITATIONS
SEE PROFILE

Mohammed Taleb Obaidat
Jordan University of Science and Technology; Jadara University
99 PUBLICATIONS **376** CITATIONS
SEE PROFILE

COMPUTER VISION-BASED TECHNIQUE TO MEASURE DISPLACEMENT IN SELECTED SOIL TESTS

Mohammed Taleb Obaidat[1], and Mousa F. Attom[2]

ABSTRACT: The potential of normal case photography using Charge-Coupled-Device (CCD) cameras to extract deformation (strain) in soil specimens of two soil tests; i.e. the unconfined compression test and the direct shear test, was investigated. A PC-based digital vision system was used to obtain accurately measured linear displacement. Using remoulded soil specimens, comparisons between displacement measurements using ASTM conventional methods and the normal case photography method showed that the use of the later method is promising and could be used as a substitute for strain gauges. Experimental investigation showed that differences between displacement measurements using conventional ASTM procedures and computer vision technique were consistently within 0.04±0.15 to 0.3±0.23 mm for unconfined compression test and direct shear test, respectively. This was compatible with the image scale where one pixel on the image domain was equivalent to about 0.4 mm on object space coordinates. Statistical correlations between strains by the two methods supported this result. Image scale and resolution were found to be the two major factors affecting the accuracy of the measurements. The results of this work are expected to open the door for geotechnical engineers and agencies responsible for soil testing standards to incorporate image-based analysis in soil testing. This will indeed bridge the gap between manual and fully automated soil testing measurements.

KEY WORDS: Computer vision, Normal case photography, Soil properties, Displacement, Strain.

INTRODUCTION

Soil testing is used to evaluate various properties of soil such as compressibility, volumetric stability, and shear strength. These properties are calculated based on displacement measured manually or by data acquisition systems.

[1]Assistant Professor of Civil Engineering, Civil Engineering Department, Jordan University of Science and Technology (J.U.S.T.), Irbid, P.O. Box 3030, Jordan.
[2]Assistant Professor of Civil Engineering, Civil Engineering Department, Jordan University of Science and Technology (J.U.S.T.), Irbid, P.O. Box 3030, Jordan.

Laboratory testing generally requires human operators. In some tests, such as unconfined compression and direct shear, it is necessary to observe the behavior of the specimen and read incremental displacements continuously with time. The measurements usually provide only a final deterministic value to the soil strength parameters without regard to the failure mechanism or to the failure plane development during the test. A geotechnical engineer must be present throughout the test duration. Moreover, human errors are ever-present. However, the test can be automated utilizing some technological trends such as computer-based data acquisition systems based on digital images.

It is sometimes desired to observe the failure plane and follow the failure mechanism in the tested soil specimen. Many methods have been reported in the literature that describe the measurement of soil deformations due to applied load. Examples of these methods include optographic trace recording (Feeser 1984) and X-ray techniques (Bouazza 1992).

Charge-Coupled-Device (CCD) video cameras as well as non-metric cameras might replace the human operator by monitoring the deformation of the tested soil samples (Faig 1976; Ayeni 1985; Gustafsson and Knutsson 1994; and Obaidat and Wong 1996-a). The image plane of the CCD camera consists of a rectangular array of sensor elements (called Sels). The physical location of each sensor element is fixed with respect to other elements. Each Sel contains a photosensitive area that is used to collect photons of light incident on the image plane. There are two major types of CCD cameras, interline transfer and frame transfer. In case of interline transfer, photosensitive areas are often less than half of the overall sensor area, whereas, it is over 90% of the surface area of the image plane in frame-transfer cameras. Therefore, frame transfer cameras tend to have much higher resolution potential (Wiley 1991). The image plane and field of view of CCD cameras are significantly smaller than that of conventional film cameras. However, the CCD camera is stable over time and has no film distortion; not like the conventional cameras. Therefore, CCD cameras

tend to have much higher measurement accuracy potential when using suitable data reduction scheme.

The cameras do not cancel the role of the operator, instead the captured images might be used for later functions, such as two or three dimensional gauging. Thus, the existence of the operator is not required if the tested specimen is located in the field of view of the used camera. Other advantages of CCD video cameras as data acquisition systems include: 1) the grabbed images of the tested specimens could provide a permanent record which can be used for measurement tasks as well as educational demonstration purposes; 2) the extracted measurements are accurate and have the potential capability of real-time (Karara and Abdel-Aziz 1974; Wong and Ho 1986; and Bouazza 1992); and 3) the method may also be adapted to in-situ measurements (Hryciw and Raschke 1996).

In stereo photogrammety applications, normal or convergent camera setups are used to extract surface deformations of the object. In the normal case, the optical axes of the stereo cameras are perpendicular to the line connecting the two exposure centers (the base) of the stereo cameras (Abdel-Aziz 1982). However, in convergent stereo photogrammetry, the optical axes of the two cameras are converted to a point located in the common area of the cameras field of view and making a convergent angle of not less than 60°. The accuracy of the object-space points in the case of convergent photography is a non-linear function of the base/object distance ratio, scale, and angle of convergence (Abdel-Aziz 1974; and Obaidat and Wong 1996-a). The positions of any unknown object points inside the common area can be found by using the corresponding image points and the computed orientation parameters of cameras at the moment of exposure. Stereo photogrammetry has been used to measure displacement fields and analyze the development of shear bands in sand (Butterfield *et al* 1970, and Harris *et al* 1995). In order to avoid the accuracy constraints of convergent photography, normal case photography was used in this research.

On the other hand, digital image techniques have been proven to be effective for volume change and micro-deformation measurements in sand (Macari-Pasqualino *et al.* 1993, and Raschke and Hryciw 1996).

The main objective of this research was to investigate the accuracy of normal case photography to measure linear deformations of soil specimens. The results of this approach were compared with conventional procedures for two soil tests; i.e. unconfined compression and direct shear tests.

NORMAL-BASED CAMERA CONFIGURATION

Normal case is the simplest and most convenient method for close-range photogrammetry mapping. The data acquisition arrangements for normal and convergent photography are shown in Figure 1. The two cameras axes are parallel and perpendicular to the base (b). Each photograph is considered as a recorder of the bundle of light rays traveling from the object points, corresponding image points, and the exposure center of the camera. The object-space coordinates (X,Y,Z) of point P could be quantified using simple geometric formulas by measuring the conjugate image point coordinates; i.e. (x_l,y_l) and (x_r,y_r), and camera base (b), and knowing the cameras focal lengths and the elevation of the camera position for one camera (Ghosh 1988). Focal lengths are determined by calibrating the cameras using any calibration procedure.

For the soil tests of concern, there is no need to compute the three-dimensional (3-D) coordinates of the points, instead a linear deformation measurement is required. Consequently, one camera is sufficient to map the tested scene from one position if this camera's optical axis is perpendicular to the (XZ) object-space plane projection for the soil specimens. This camera setup produces a constant scale for a flat-mapped scene or a line parallel to any object-space axis. Thus, it was utilized in this research work. The camera motion was constrained to parallel movement and

scale uniformity was controlled by setting-up the camera on a tripod equipped with a manual levelling unit.

A square (of 10x10 cm) having a black color line marking, was drawn on a white paper in order to have different intensity backgrounds. The object-space and image lengths of each side of the square were used to compute the image scale in both the vertical and horizontal directions. Once the scale and the length of any portion on the image at any time is known, the object spatial displacement can be computed.

COMPUTER VISION SYSTEM

A low resolution Samsong CCD camera, which is available in the PC-based vision system laboratory at Jordan University of Science and Technology, was used to acquire image data for the tested specimens. The available computer vision hardware system consists of a Personal Computer (PC) equipped with a digitizing board and a video monitor used to display digital images. The system usage was restricted to freeze image frames at regular intervals of 15 seconds to compute strain readings of soil specimens.

The camera zoom lens was fixed at a focal setting of about 25 mm (1 mm is equivalent to about 94.5 pixels) to control the camera field of view. To assure the effectiveness of the proposed approach, the used camera was calibrated using a planar wall to define its interior geometry; i.e. the effective focal length in pixels, radial and decentering lens distortion parameters, and the affine scaling parameter. This calibration method proved to be effective for determining the geometric distortions along the directions of the rows and the columns of the digital image (Obaidat and Wong 1996-b). The camera was close enough to the tested soil specimens to increase the image scale. The distance between the camera and the tested soil specimen was less than one meter. The tested specimens were approximately centered in the middle of the image for two reasons: 1) minimizing the distortion effect; and 2) assuring mapping scale uniformity.

Digital images were captured using a standard monochrome Phase Alternation Line (PAL) system format of 752Hx480V pixels (one pixel is about 0.02 μm in the image domain). Image frames were digitized at 256 gray levels using a PC equipped with a frame-grabber board. The video monitor was used to display the captured image frames. The image was then saved as a binary format file.

Image coordinates were measured using computer software developed specifically for this research work. The software works under MS-Windows environment and has the capability to display individual images and extract their coordinates to a sub-pixel accuracy. Measured image coordinates were then refined to correct for decentering and radial distortions of the camera lens using the correction model shown in the following equations (Fryer, 1989):

$$\text{Corrected}(x_{ij}) = x_{ij} + dx_{ij} \quad (1)$$

$$\text{Corrected}(y_{ij}) = y_{ij} + dy_{ij} \quad (2)$$

where:

x_{ij} and y_{ij} are the measured image point coordinates of point j on photograph i,

dx_{ij} and dy_{ij} are their corresponding corrections for distortion effect of image point j at photograph i, where:

$$dx_{ij} = \bar{x}_{ij}\left[L_1 r_{ij}^2 + L_2 r_{ij}^4 + L_3 r_{ij}^6 + L_4 r_{ij}^8\right] + \left[P_1(r_{ij}^2 + 2\bar{x}_{ij}^2) + 2P_2 \bar{x}_{ij}\bar{y}_{ij}\right]\left[1 + P_3 r_{ij}^2\right] \quad (3)$$

$$dy_{ij} = \bar{y}_{ij}\left[L_1 r_{ij}^2 + L_2 r_{ij}^4 + L_3 r_{ij}^6 + L_4 r_{ij}^8\right] + \left[P_2(r_{ij}^2 + 2\bar{y}_{ij}^2) + 2P_1 \bar{x}_{ij}\bar{y}_{ij}\right]\left[1 + P_3 r_{ij}^2\right] \quad (4)$$

$$\bar{x}_{ij} = (x_{ij} - x_p)(1 + k) \quad (5)$$

$$\bar{y}_{ij} = (y_{ij} - y_p) \quad (6)$$

$$r_{ij} = \sqrt{(\bar{x}_{ij} + \bar{y}_{ij})} \quad (7)$$

x_p, y_p = image coordinates of the principal point,

f = focal length,

L_1, L_2, L_3, L_4 = parameters of radial lens distortion. Radial distortion is symmetric about the principal point of symmetry and is a function of distance from that point. The quality of the lens and the format size of the camera normally control the number of terms carried in the calibration solution.

P_1, P_2, P_3 = parameters of asymmetric distortion. Decentering distortion is introduced as a result of imperfect assembly of lens elements. The result of this imperfect centration of lens elements is a combined tangential and asymmetrical radial displacement of the image.

k = affine scale parameters.

EXPERIMENTAL RESULTS

The methodology presented before was used to investigate the accuracy and effectiveness of normal-based images to extract displacement measurements for both direct shear test and unconfined compression test. American Standard for Testing and Materials (ASTM) standard procedures were also used to quantify linear displacement for the purpose of comparison between the two approaches.

Soil Samples

A disturbed soil sample was obtained from the eastern part of Irbid city, Jordan, at one meter depth below the natural ground surface and tested at the soil mechanics laboratory of the Civil Engineering Department, Jordan University of Science and Technology (J.U.S.T.), Jordan. The physical properties of the soil was determined in accordance with the ASTM standards. These properties included Atterberg's limit (ASTM D4318), composition (ASTM D422), maximum dry density (ASTM D1557), and optimum moisture content (ASTM D1557). Table 1 shows the different physical properties of the soil used.

A) Conventional Procedures

The Unconfined Compression Test (ASTM D2166)

The unconfined compressive strength of the soil is defined as the maximum stress obtained from the stress strain relation in the unconfined compression test. In this test, the specimens were remoulded at 95% relative compaction from the standard proctor density test in the standard compaction mold at the optimum water content with the dimension of 1.6 inch (4.06 cm) in diameter and 3.2 inch (8.12 cm) in height. The specimens were then placed in the unconfined compression device for shearing at a strain rate of 0.8 mm/minute. The shearing load with its correspondent deformation was recorded until a failure in the specimen was observed. Four readings were taken after the failure took place. The unconfined compressive strength of the tested specimen was 178 kN/m^2.

The Direct Shear Test (ASTM D3080)

Three identical specimens were tested. All specimens were prepared in accordance with the ASTM direct shear mold at 95% relative compaction from the standard proctor density test and at the optimum water content. The specimen dimensions were 5.1x5.1 cm. The specimens were placed in the direct shear device with displacement shearing rate about 0.16 cm/minute under three different normal loads. The shearing load and the horizontal deformation were recorded until failure. The shear stresses were found to be 59.3, 89.4, and 120.2 kN/m^2 for the correspondent normal stresses of 75.4, 150.8, and 226.2 kN/m^2, respectively.

B) Normal-Based Camera Vision Approach

A square having dimensions of 10x10 cm, drawn on a piece of paper, was used in the background of the tested specimens for purpose of scaling actual dimensions from captured video images. The uniform scale of normal photography can be known when knowing the actual length of the square in mm and measuring the square length in image domain in pixels. This gives the scale equivalency of a pixel in mm. For both tests, normal-based images for tested specimens were captured every 15 seconds for a period of nine minutes until failure. The square (to be called scale-

square) drawn on a piece of paper always appeared in the images for purpose of computing image scale. Figures 2 shows specimens of normal-based digital images for the unconfined compression test at the beginning of the test (time zero) and at the failure stage (after about nine minutes).

Digital image coordinates were measured using the upper left corner of the image as coordinates system origin (0,0). x-axis of the image was positive to the right, while the y-axis was positive downward. It is worthwhile mentioning here that, the measured displacement in the case of the unconfined compression test was vertical; i.e. y-axis image coordinates, while it was horizontal in case of direct shear test; i.e. x-axis image coordinates. The camera distance from the tested specimens was kept approximately the same for both tests in order to produce a uniform scale. The length or width of scale-square was about 244 pixels for both tests. One pixel in the image domain was equivalent to about 0.02 μm. The upper and lower y-coordinates on the image domain for the two edges of the tested specimen was measured in the unconfined compression test, while the x-coordinates of the left edge and a fixed point on the right side of the image was measured in the direct shear test. The upper edge coordinate was constant because it was not moved while performing the unconfined compression test, while the right edge coordinate was not changed in the case of the direct shear test for the same reason.

Linear displacements as a function of time were computed (scaled) for the unconfined compression test and the direct shear test according to the following equation:

$$\varepsilon_i = H - l\,(\Delta_i/\Delta_s) \qquad (8)$$

where:

ε_i = linear displacement at time i (in mm);

H = initial length of specimen (in mm);

l= length or width of scale-square in mm (i.e., it is constant quantity and equals 100 mm);

Δ_i= difference between coordinates of the edges of the soil specimen at time *i (*in pixels). It is variable with time; and

Δ_s= difference between coordinates of the scale-square edges (in pixels);

The difference between coordinates of the edges of the soil specimen at time *i* in pixels was the difference between the y-coordinates of the upper and lower edges of the soil specimen in case of unconfined compression test, while it was the difference between the x-coordinates of the left and right edges in case of direct shear test.

Tables 2 and 3 show the results of extracted linear displacements as functions of time for both the unconfined compression test and direct shear test, respectively. As shown, the procedures are quite simple and require measurement of only two image coordinates for each tested specimen in order to measure strain at a certain time. Figures 3 and 4 show the measured linear displacements using both the conventional and vision approaches for both unconfined compression test and direct shear test, respectively. From the figures, it is clear that minor differences exist between the two methods. The mean errors for 37 displacement measurements using the two methods were 0.044±0.150 mm and 0.038±0.023 cm for the unconfined compression test and the direct shear test, respectively. The summations for the differences of the 37 measurements were 1.639 mm and 1.41 cm for the unconfined test and the direct shear test, respectively.

The measured displacements of the unconfined test by conventional and computer vision techniques were correlated to give the following linear equation:

$$Y_1 = 0.967X_1 + 0.1615 \qquad R^2 = 0.9963 \qquad (9)$$

where:

Y_1= displacement using conventional method (mm); and

X_1= displacement using vision technique (mm).

Residual sum of squares was 0.618.

Similar equation was also found for direct shear test:

$$Y_2 = 1.013X_2+0.0294 \qquad R^2 = 0.9975 \qquad (10)$$

where:

Y_2= displacement using conventional method (cm); and

X_2= displacement using vision technique (cm).

Residual sum of squares was 0.01708.

Obviously, high and consistent correlations exist in the previous two equations. The slopes of the equations were almost equal to one. This is an indication of the high accuracy of computer vision measurements. Consequently, computer vision technique could be used as an alternative to conventional procedures in order to quantify linear displacement for the two mentioned soil tests.

CONCLUSIONS

Computer vision technology has been successfully used to quantify displacement (strain) measurements for two soil tests; the unconfined compression test and the direct shear test. For both tests, differences between displacement measurements using conventional ASTM procedures and computer vision technique were consistently within 0.04±0.15 to 0.30±0.23 mm, respectively. Statistical correlations between the results of conventional tests procedures and vision method supported this conclusion. The accuracy of the measurements was also consistent with the image-scale. 244 pixels in image domain were equivalent to 100 mm in object space coordinates; i.e. one pixel was equal to about 0.4 mm in object-space coordinates. Consequently, enhancing the camera resolution and/or increasing the image scale will give better results. The results showed that the use of computer vision technology to measure linear displacements for tested soil specimens had a considerable potential capability which makes it indeed a realistic possibility to substitute the process of strain gauges visualization.

Geotechnical engineers and agencies responsible for soil testing standards are encouraged to incorporate the use of normal case cameras in order to measure deformations and strains as well as

visualize the failure shape in soil specimens. Reasons behind that are due to accuracy potentials of computer vision technology, permanent record and durable testing visualization, and capability of real-time potential and performing in-situ surface measurements. It is worthwhile mentioning here that, the potential of the proposed computer vision technique can most fully be exploited if further research is directed to extract three-dimensional (3-D) surface deformation of the tested soil specimens. This work requires two normal-based cameras; i.e. stereo vision. One of the expected advantages of this method is that it may give an indication to understand the behavior of the soil specimens at the failure stage.

The average cost of the described measurement system including vision system with a CCD camera is less than 4000 U.S. dollars which is relatively a low cost system. The basic methodology of the proposed computer vision technique to extract linear and surface measurements may be extended to numerous other soil tests including: permeability, consolidation, swelling, etc. The numerous measurement applications of the proposed system are anticipated to support the feasibility and potential of ASTM adopting the system's procedure as a standard test procedure.

REFERENCES

Abdel-Aziz, Y. I. "Expected Accuracy of Convergent Photos", *Photogrammetric Engineering*, Vol. 40, 1974, pp. 1341-1346.

Abdel-Aziz, Y. I. "Accuracy of the Normal Case of Close-Range Photogrammetry", *Photogrammetric Engineering and Remote Sensing*, Vol. 48, No. 2, 1982, pp. 207-213.

Ayeni, O. O. "Photogrammetry as a Tool for National Development", *Photogrammetric Engineering and Remote Sensing*, Vol. 51, No. 4, 1985, pp. 445-454.

Bouazza, A. “The Use of the Stereo-Photogrammetry Method in Geotechnical Engineering Work”, *International Archives of Photogrammetry and Remote Sensing (ISPRS*), Vol. XXIX, Commission V, Part B5, ISPRS, Washington, D.C., 1992, pp. 160-164.

Butterfield, R., Harkness, R. M., and Andrawes, K. Z. “A Stereophotogrammetric Method for Measuring Displacement Fields”, *Geotechnique*, Vol. 20, No. 3, 1970, pp. 308-314.

Faig, W. “Photogrammetric Potentials of Non-Metric Cameras”, *Photogrammetric Engineering and Remote Sensing*, Vol. 42, No. 1, 1976, pp. 47-49.

Feeser, V. “Optographic Trace Recording: A New Method of Strain Measurement in Geotechnical Testing”, *Geotechnique*, Vol. 34, No. 2, 1984, pp. 277-281.

Fryer, J. G. "Camera Calibration in Non-Topographic Photogrammetry", *Non-Topographic Photogrammetry, 2nd Ed., American Society for Photogrammetry and Remote Sensing,* Fall Church, VA, 1989, pp. 59-70

Ghosh, S. K. “Analytical Photogrammetry”, Second Edition, *Pergamon Press*, New York, U.S.A., 1988, 308 pages.

Gustafsson, L., and Knutsson, S. “An Image Analysis Method for Studying the Movements in Granular and Solid Bodies”, ASTM Geotechnical Testing Journal, Vol. 17, No. 1, 1994, pp. 95-100.

Harris, W. W., Viggiani, G., Mooney, M. A., and Finno, R. J. “Use of Stereophotogrammetry to Analyze the Development of Shear Bands in Sand”, ASTM Geotechnical Testing Journal, Vol. 18, No. 4, 1995, pp. 405-420.

Hryciw, R. D.; and Raschke, S. A. “Development of A Computer Vision Technique for In-Situ Soil Characterization”, *In Emerging Technologies in Geotechnical Engineering, Transportation Research Record,* No. 1526, 1996, pp. 86-97.

Karara, H. M.; and Abdel-Aziz, Y. I. “Accuracy Aspects of Non-Metric Imageries”, *Photogrammetric Engineering*, Volume 40, 1974, pp. 1107-1117.

Macari-Pasqualino, E. J., Costes, N. C., and Parker, J. K. “Digital Image Techniques for Volume Change Measurements in Triaxial Tests”, Proceedings of a Conference on Digital Image Processing: Techniques and Application in Civil Engineering, ASCE, 1993, pp. 211-219.

Obaidat, M. T. M.; and Wong, K. W. “Automated Knowledge-Based System for Stereo Video Metrology”, *American Society of Civil Engineers (ASCE), Surveying Engineering Division*, Vol. 122, No. 2, 1996-a, pp. 47-64.

Obaidat, M. T. M.; and Wong, K. W. “Geometric Calibration of CCD Camera Using Planar Object”, *American Society of Civil Engineers (ASCE), Surveying Engineering Division*, Vol. 122, No. 3, 1996-b, pp. 97-113.

Raschke, S. A., and Hryciw, R. D. “Micro-Deformations in Sands by Digital Image Processing and Analysis”, *in Small-Magnitude Measurements in Geotechnical Engineering*, *Transportation Research Record,* No. 1548, 1996, pp. 31-37.

Wiley, A. G. “Metric Aspects of Zoom Vision”, Ph.D. dissertation, *University of Illinois at Urbana-Champaign*, Urbana, Illinois, 1991, 159 pages.

Wong, K. W.; and Ho, W. “Close-Range Mapping with a Solid State Camera”, *Photogrammetric Engineering and Remote Sensing*, Vol. 52, No. 1, 1986, pp. 67-74.

LIST OF FIGURES

LIST OF TABLES

Table 1: Physical Properties of Soil.

Consistency Limits	
Liquid Limit	68%
Plastic Limit	32%
Plastic Index (PI)	34%
Gradation	
Sand	17%
Silt	30%
Clay	53%
$\gamma_{dmax.}$ (Maximum dry density)	13.1 KN/m^3
$W_{op.}$ (Optimum moisture content)	29%

Table 2. Results of unconfined compression test.

Time (Seconds)	Square Coordinates (Pixels) (for scale reference)			Sample Coordinates (Pixels)			Computed Sample length from Vision (cm)	Displac. from vision (mm)	Displacement from conventional procedure (mm)
	Upper	Lower	Length	Upper	Lower	Length			
15	183	427	244	209	410	201	8.24	0.00	0.20
30	183	427	244	209	409	200	8.20	0.40	0.40
45	183	427	244	209	409	200	8.20	0.40	0.60
60	183	427	244	209	408	199	8.16	0.80	0.80
75	183	427	244	209	408	199	8.16	0.80	1.00
90	183	427	244	209	407	198	8.12	1.20	1.20
105	183	427	244	209	407	198	8.12	1.20	1.40
120	183	427	244	209	406	197	8.08	1.60	1.60
135	183	427	244	209	406	197	8.08	1.60	1.80
150	183	427	244	209	405	196	8.04	2.00	2.00
165	183	427	244	209	405	196	8.04	2.00	2.20
180	183	427	244	209	405	196	8.04	2.00	2.40
195	183	427	244	209	404	195	7.99	2.50	2.60
210	183	427	244	209	404	195	7.99	2.50	2.80
225	183	427	244	209	403	194	7.95	2.90	3.00
240	183	427	244	209	402	193	7.91	3.30	3.20
255	183	427	244	209	402	193	7.91	3.30	3.40
270	183	427	244	209	401	192	7.87	3.70	3.60
285	183	427	244	209	401	192	7.87	3.70	3.80
300	183	427	244	209	400	191	7.83	4.10	4.00
315	183	427	244	209	400	191	7.83	4.10	4.20
330	183	427	244	209	399	190	7.79	4.50	4.40
345	183	427	244	209	399	190	7.79	4.50	4.60
360	183	427	244	209	398	189	7.75	4.90	4.80
375	183	427	244	209	398	189	7.75	4.90	5.00
390	183	427	244	209	397	188	7.71	5.30	5.20
405	183	427	244	209	397	188	7.71	5.30	5.40
420	183	427	244	209	396	187	7.66	5.80	5.60
435	183	427	244	209	396	187	7.66	5.80	5.80
450	183	427	244	209	396	187	7.66	5.80	6.00
465	183	427	244	209	395	186	7.62	6.20	6.20
480	183	427	244	209	395	186	7.62	6.20	6.40
495	183	427	244	209	394	185	7.58	6.60	6.60
510	183	427	244	209	393	184	7.54	7.00	6.80
525	183	427	244	209	392.5	183.5	7.52	7.20	7.00
540	183	427	244	209	392	183	7.50	7.40	7.20

Table 3. Results of direct shear test.

Time (Seconds)	Reference Coordinates (Pixels)		Measured Reference Coordinates Length using Vision (Pixels) (1 cm = about 244 pixels)	Measured Reference Coordinates Length using Vision (cm)	Measured Displac. using Vision (cm)	Measured Displacement using Conventional Procedure (cm)
	Left Side	Right Side				
15	281	316	35	1.43	0.00	0.04
30	283	316	33	1.35	0.08	0.08
45	283	316	33	1.35	0.08	0.12
60	284	316	32	1.31	0.12	0.16
75	285	316	31	1.27	0.16	0.20
90	286	316	30	1.23	0.20	0.24
105	287	316	29	1.19	0.24	0.28
120	288	316	28	1.15	0.28	0.32
135	289	316	27	1.11	0.32	0.36
150	290	316	26	1.07	0.36	0.40
165	291	316	25	1.03	0.40	0.44
180	292	316	24	0.98	0.44	0.48
195	293	316	23	0.94	0.48	0.52
210	294	316	22	0.90	0.52	0.56
225	295	316	21	0.86	0.56	0.60
240	296	316	20	0.82	0.60	0.64
255	297	316	19	0.78	0.64	0.68
270	298	316	18	0.74	0.68	0.72
285	299	316	17	0.69	0.72	0.76
300	300	316	16	0.65	0.76	0.80
315	301	316	15	0.61	0.80	0.84
330	302	316	14	0.57	0.84	0.88
345	303	316	13	0.53	0.88	0.92
360	304	316	12	0.48	0.92	0.96
375	305	316	11	0.44	0.96	1.00
390	306	316	10	0.40	1.00	1.04
405	307	316	9	0.36	1.08	1.08
420	308	316	8	0.32	1.12	1.12
435	309	316	7	0.28	1.16	1.16
450	310	316	6	0.24	1.20	1.20
465	310	316	6	0.24	1.20	1.24
480	311	316	5	0.20	1.24	1.28
495	312	316	4	0.16	1.27	1.32
510	312	316	4	0.16	1.27	1.36
525	313	316	3	0.12	1.31	1.40
540	314	316	2	0.08	1.34	1.44

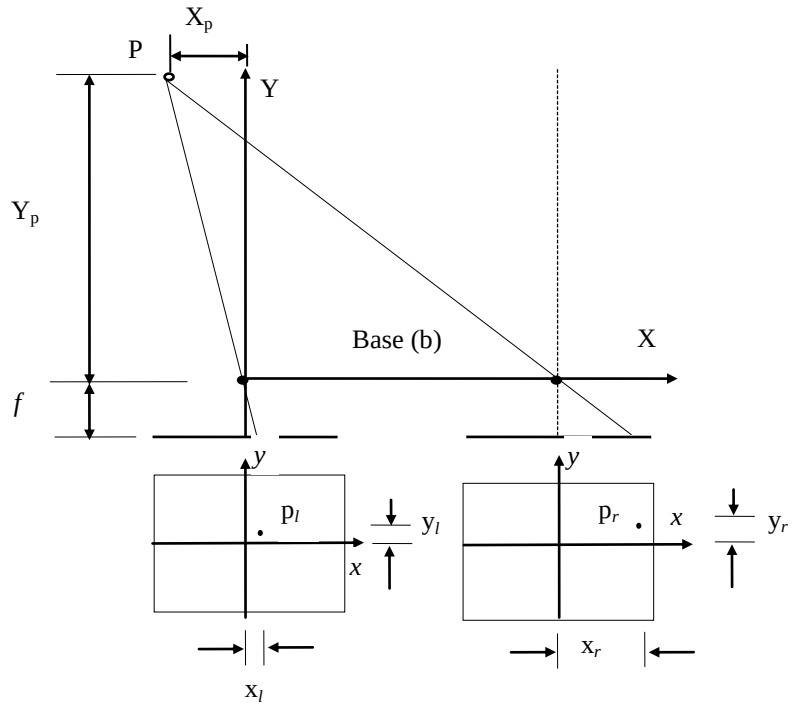

Figure 1: Data acquisition arrangement for normal case photography.

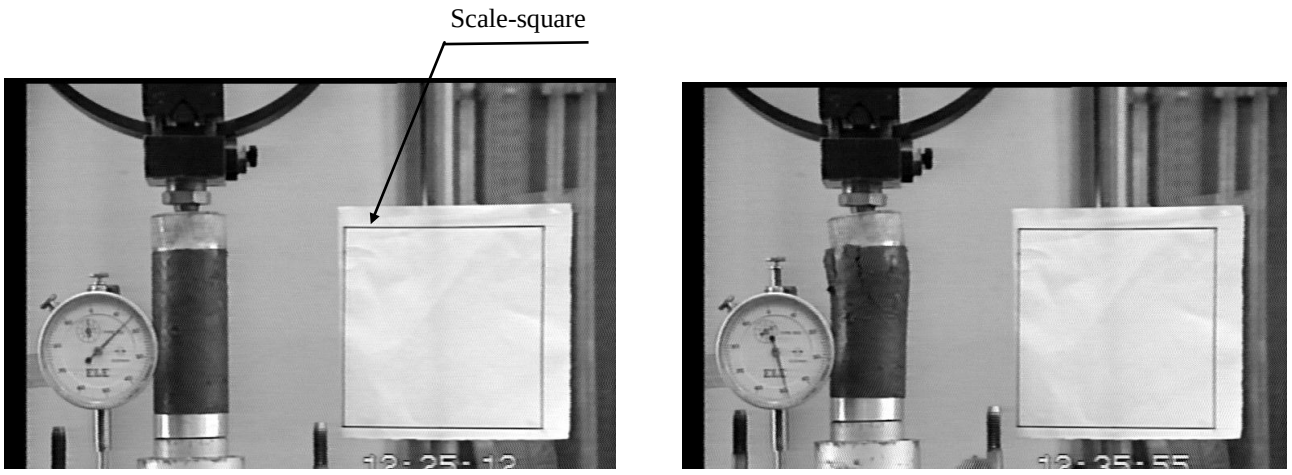

a. time zero b. failure stage

Figure 2: Samples of normal case digital images for the unconfined test at the beginning of the test (time zero) and at the failure stage (after about nine minutes).